BIOLOGY OF REPRODUCTION (2012) **86**(6):174, 1–15
Published online before print 7 March 2012.
DOI 10.1095/biolreprod.112.099176

Overactivation of Hedgehog Signaling Alters Development of the Ovarian Vasculature in Mice[1]

Yi Ren,[3] Robert G. Cowan,[3] Fernando F. Migone, and Susan M. Quirk[2]

Department of Animal Science, Cornell University, Ithaca, New York

ABSTRACT

The hedgehog (HH) signaling pathway is critical for ovarian function in *Drosophila*, but its role in the mammalian ovary has not been defined. Previously, expression of a dominant active allele of the HH signal transducer protein smoothened (SMO) in *Amhr2*$^{cre/+}$*SmoM2* mice caused anovulation in association with a lack of smooth muscle in the theca of developing follicles. The current study examined events during the first 2 wk of life in *Amhr2*$^{cre/+}$*SmoM2* mice to gain insight into the cause of anovulation. Expression of transcriptional targets of HH signaling, *Gli1*, *Ptch1,* and *Hhip*, which are used as measures of pathway activity, were elevated during the first several days of life in *Amhr2*$^{cre/+}$*SmoM2* mice compared to controls but were similar to controls in older mice. Microarray analysis showed that genes with increased expression in 2-day-old mutants compared to controls were enriched for the processes of vascular and tube development and steroidogenesis. The density of platelet endothelial cell adhesion molecule (PECAM)-labeled endothelial tubes was increased in the cortex of newborn ovaries of mutant mice. Costaining of preovulatory follicles for PECAM and smooth muscle actin showed that muscle-type vascular support cells are deficient in theca of mutant mice. Expression of genes for steroidogenic enzymes that are normally expressed in the fetal adrenal gland were elevated in newborn ovaries of mutant mice. In summary, overactivation of HH signaling during early life alters gene expression and vascular development and this is associated with the lifelong development of anovulatory follicles in which the thecal vasculature fails to mature appropriately.

follicular development, ovary, ovulation

INTRODUCTION

Ovarian follicle formation and development involve remodeling events that are common to many tissues and that are often regulated by families of developmental signaling pathways including wingless-related MMTV integration site (WNT), transforming growth factor-β (TGFB), fibroblast growth factor (FGF), notch, and hedgehog (HH). The overall goal of the present study was to examine the role of the HH signaling pathway in early follicle development in the mouse. The HH pathway regulates embryonic development as well as the function of adult tissues through effects on cell proliferation, differentiation, and survival [1]. In mammals, the HH signaling pathway consists of three ligands, sonic, Indian, and desert HH (SHH, IHH, and DHH); the membrane receptor patched (PTCH1); and the transmembrane signal transducer protein smoothened (SMO). In the absence of ligand binding, PTCH1 maintains SMO in an inactive state. Binding of one of the ligands to PTCH1 relieves inhibition of SMO and signaling occurs through downstream transcription factors, GLI1, GLI2, and GLI3 [2].

In order to investigate the role of HH signaling in the ovary, we created mice in which a dominant active allele of SMO, known as SMOM2, is conditionally expressed in the ovary [3]. SMOM2 has a point mutation that prevents its negative regulation by PTCH1 [4, 5]. In *Amhr2*$^{cre/+}$*SmoM2* mutant mice, CRE-mediated recombination in somatic cells of the ovary removes a loxP-flanked stop codon and thereby activates expression of a *SmoM2*/yellow fluorescent protein (*Yfp*) fusion gene. We previously reported that *Amhr2*$^{cre/+}$*SmoM2* mice are infertile; although follicles develop to preovulatory status and undergo many of the changes expected in response to an LH surge, they fail to rupture at the time of ovulation, and luteinization proceeds around trapped oocytes [3]. The major difference detected in mutant mice is that the theca layer of growing follicles expresses reduced levels of genes associated with smooth muscle and lacks smooth muscle actin-α (SMA)-positive cells. Interestingly, HH target genes are expressed at similar levels in preovulatory follicles of mutant and control mice, suggesting that the anovulatory phenotype in mutant mice may be caused by overactivation of HH signaling at relatively early stages of ovarian and follicle development [3].

During the first 4 days of life in the mouse and rat, cord structures consisting of oocytes and somatic cells enclosed by a basement membrane break down and are remodeled to form primordial follicles [6, 7]. Some primordial follicles begin to grow immediately, leading to the presence of small numbers of primary follicles on Days 0–4 that contribute to the first wave of follicle development. HH signaling appears to be activated as primordial follicles leave the resting stage and begin to grow; DHH and IHH are produced by granulosa cells of primary and larger follicles, and expression of transcriptional targets of HH signaling, including *Gli1*, *Ptch1*, and *Hhip*, is enriched in mesenchymal cells immediately surrounding follicles and in the theca cell layer [3, 8, 9]. The current study identified events during the first several weeks of life that were altered by overactivation of HH signaling and that may contribute to the anovulatory phenotype in *Amhr2*$^{cre/+}$*SmoM2* mutant mice.

MATERIALS AND METHODS

Mouse Strains and Management

Amhr2$^{cre/+}$ mice were provided by Dr. Richard Behringer [10] and *GT(ROSA)26Sor*$^{tm1(smo/YFP)Amc}$ mice [5] carrying the *SmoM2* allele were

[1]Supported by the Eunice Kennedy Shriver National Institute of Child Health and Human Development grant R03HD057648 (to S.M.Q.), Research Initiation Award 0547373 (to S.M.Q.) from the National Science Foundation ADVANCE Institutional Transformation to Cornell University, and the Center for Vertebrate Genomics, Cornell University (to S.M.Q). Microarray data were deposited to GEO under the accession number GSE35123.
[2]Correspondence: Susan M. Quirk, Department of Animal Science, 434 Morrison Hall, Cornell University, Ithaca, NY 14853.
E-mail: smq1@cornell.edu
[3]These authors contributed equally to this work.

Received: 16 January 2012.
First decision: 5 February 2012.
Accepted: 23 February 2012.

eISSN: 1529-7268 http://www.biolreprod.org
ISSN: 0006-3363

TABLE 1. Quantitative real-time RT-PCR assays.

Gene symbol	Gene name	Assay ID[a]	Exons[b]
Dhh	Desert hedgehog	Mm00432820_m1	2–3
Ihh	Indian hedgehog	Mm00439613_m1	2–3
Shh	Sonic hedgehog	Mm00436527_m1	1–2
Ptch1	Patched homolog 1	Mm00436026_m1	17–18
Hhip	Hedgehog-interacting protein	Mm00469580_m1	12–13
Gli1	GLI-Kruppel family member GLI1	Mm00494645_m1	2–3
Gli2	GLI-Kruppel family member GLI2	Mm01293117_m1	8–9
Gli3	GLI-Kruppel family member GLI3	Mm00492333_m1	1–2
Smo	Smoothened homolog	Mm01162710_m1	8–9
Star	Steroidogenic acute regulatory protein	Mm00441558_m1	3–4
18s rRNA		4319413E	

[a] Taqman Gene Expression Assays (Applied Biosystems).
[b] Exons in which forward and reverse primers anneal.

purchased from the Jackson Laboratory. Male *Amhr2*$^{cre/+}$ mice and female *GT(ROSA)26Sor*$^{tm1(smo/YFP)Amc}$ mice were mated to obtain *Amhr2*$^{cre/+}$*SmoM2* mice (mutants) and *Amhr2*$^{+/+}$*SmoM2* mice (controls). Mice were genotyped from tail DNA using protocols provided by the Jackson Laboratory. Mice were maintained in accordance with the NIH *Guide for the Care and Use of Laboratory Animals*. Studies were approved by the Cornell University Institutional Animal Care and Use Committee.

YFP Expression

YFP expressed from the *SmoM2-Yfp* allele was examined using a Zeiss LSM 510 confocal microscope (Carl Zeiss Microimaging). Ovaries were fixed in 4% paraformaldehyde (PFA) for 1 h, rinsed in PBS, mounted in aqueous mounting media, and examined within 24 h. YFP was excited at 514 nm and viewed using a 520–550-nm band-pass filter.

Real-Time RT-PCR Analysis of Gene Expression

RNA was prepared from whole ovaries using a RNeasy Micro Kit (Qiagen). Reverse transcription was performed using a High Capacity cDNA Reverse Transcription Kit (Applied Biosystems). Real-time RT-PCR was performed on an ABI Prism 7000 (Applied Biosystems) using the mouse-specific assays listed in Table 1. A standard curve used in each assay was constructed by serial dilution of cDNA prepared from a RNA pool of immature (21- to 23-day-old) mouse ovaries. In assays for each gene, values for samples were standardized by dividing by the value of the corresponding 18S rRNA and multiplying by 100. For each gene analyzed, all samples were assayed on the same plate.

In Situ Hybridization

Whole-mount in situ hybridization for *Ptch1*, *Gli1*, and *Hhip* were performed using previously described probes [11–13]. Tissues were fixed in 4% PFA and stored at −20°C in 100% methanol. Antisense probes were labeled with digoxigenin (DIG) using a commercial kit (Roche Bioscience). Following bleaching with 4.5% H_2O_2, rehydration, and permeabilization, tissues were incubated overnight at 68°C with either antisense riboprobe or no probe. Tissues were washed and incubated with alkaline phosphatase-conjugated anti-DIG antibody and signal detected using BM purple substrate (Roche Bioscience) followed by fixation in 4% PFA. Tissues were embedded in 5% low-melt agarose and 15-μm-thick sections cut with a vibratome. Nuclei were counterstained with 1 μg/ml propidium iodine. Color images of BM purple staining were overlaid on fluorescent images of propidium iodide to assist in localization of RNA signals; identical settings and adjustments were used for all images for each probe.

Microarray Analysis

RNA was prepared from ovaries of 2-day-old *Amhr2*$^{+/+}$*SmoM2* control and *Amhr2*$^{cre/+}$*SmoM2* mutant mice using a RNeasy Mini Kit (Qiagen). Each sample consisted of RNA from 16 ovaries from 8 mice. RNA quality was assessed by measurement of ribosomal RNA on an Agilent 2100 Bioanalyzer (Agilent Technologies). Microarray analyses were performed by the Microarray Core Facility of the Cornell University Life Sciences Core Laboratories Center using Affymetrix GeneChip Mouse Genome 430v2 chips (Affymetrix). Raw array data was processed by Affymetrix GCOS software to obtain signal values. The signal values were log2-transformed after being offset by +64, and fold differences were calculated as the difference between mutant and control samples. Only probe sets having at least one Present call were included in the analyses described in the *Results* section.

Histology and Immunohistochemistry

Ovaries were fixed in Bouin fixative and stained with hematoxylin and eosin (H&E) for histology or fixed in 2% PFA for immunohistochemistry and stored in ethanol at 4°C. Tissues were embedded in paraffin and 5-μm sections

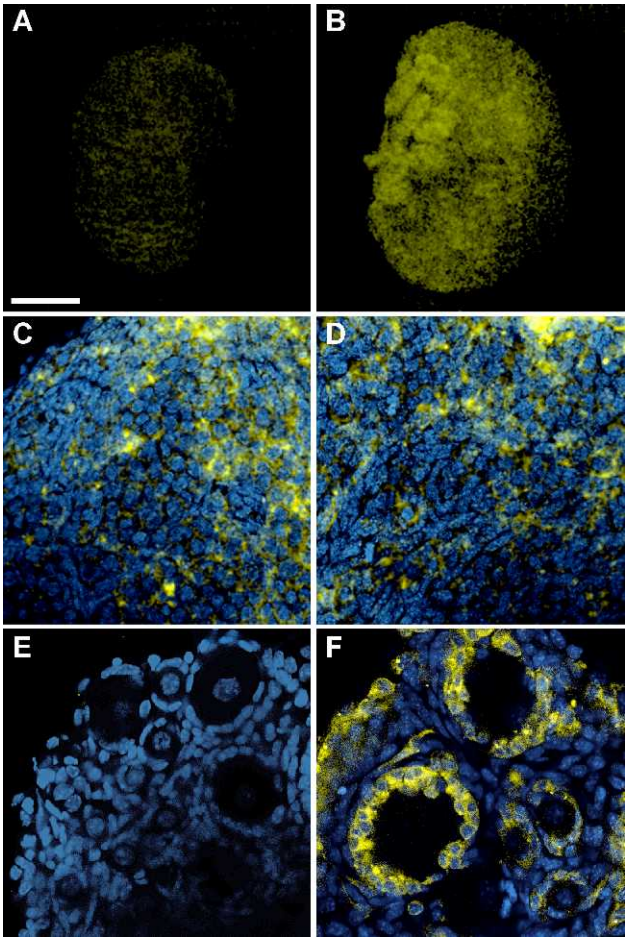

FIG. 1. Expression of the SMOM2/YFP fusion protein examined by confocal microscopy of whole-mount ovaries from *Amhr2*$^{+/+}$*SmoM2* control and *Amhr2*$^{cre/+}$*SmoM2* mutant mice on the day of birth (**A**–**D**) and at Day 10 of age (**E**, **F**). Images of control ovaries are shown in **A** and **E** and all other panels show images of mutant ovaries. **C** and **D** show higher-power images of cortex and medulla, respectively, of the ovary shown in **B**. Bar in **A** = 200 μm for **A** and **B** and 40 μm for **C**–**F**.

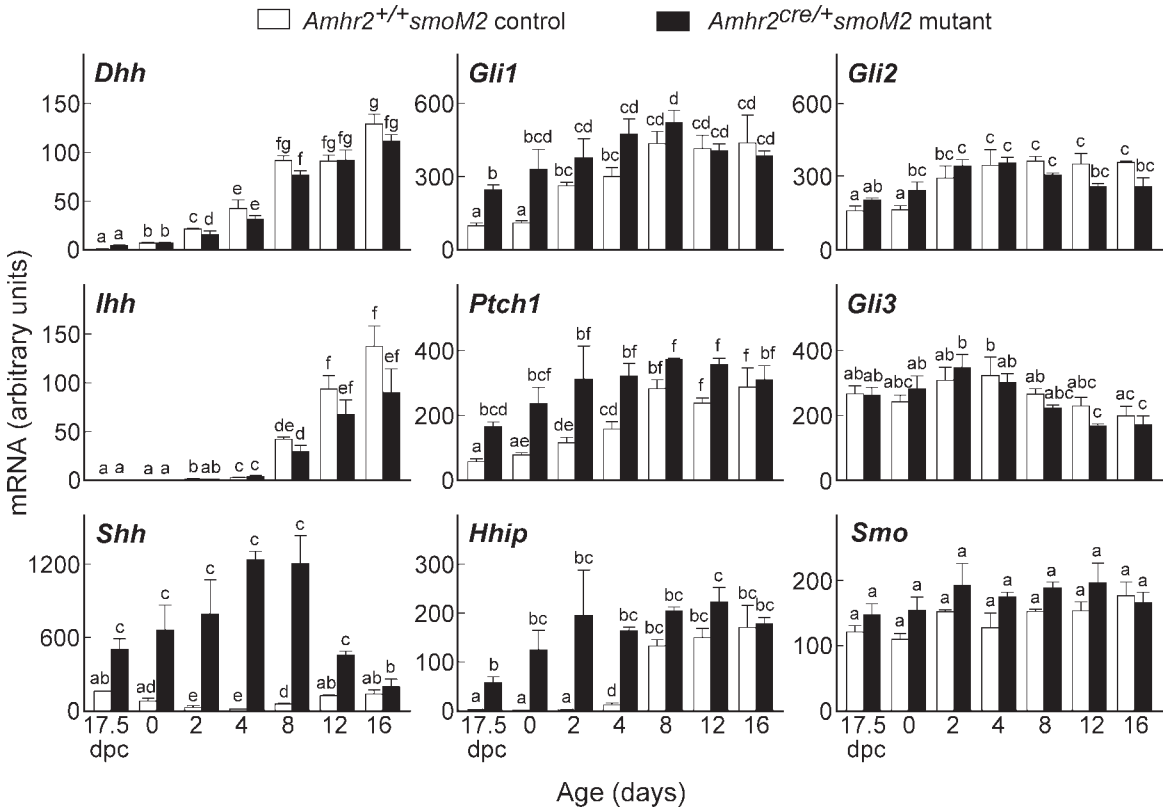

FIG. 2. Developmental pattern of expression of genes in the HH signaling pathway in ovaries of *Amhr2*$^{+/+}$*SmoM2* control and *Amhr2*$^{cre/+}$*SmoM2* mutant mice. Ovaries obtained from mice of various ages were pooled to obtain sufficient quantities of RNA (three mice at 17.5 dpc and 0, 2, and 4 days of age; 2 mice at 8, 12, and 16 days of age). Total RNA was assayed by quantitative real-time RT-PCR. Data are mean ± SEM (n = 3 RNA preparations). Within each panel, bars without common superscripts are significantly different ($P < 0.05$).

prepared. For CYP17A and CYP21A immunohistochemistry, antigen retrieval was performed in citric acid buffer (pH 5.0) and sections were blocked with 2% normal goat serum (NGS). Sections were incubated overnight at 4°C with rabbit anti-bovine CYP17A diluted 1:200 (obtained from Dr. Alan J. Conley, University of California at Davis), rabbit anti-human CYP21A diluted 1:2500 (obtained from Dr. Walter L. Miller, University of California at San Francisco), or, as controls, normal rabbit serum diluted 1:200 or 1:2500 in PBS-1% bovine serum albumin (BSA). Sections were washed and incubated with 0.5 μg/ml Alexa 488 goat anti-rabbit IgG (Invitrogen) in PBS-1% BSA for 4 h at room temperature and then counterstained with 1 μg/ml Hoechst 33342. Fluorescence was viewed using a Nikon Diaphot 300 microscope (Nikon Instruments), and images were obtained using a Spot II Digital Camera (Diagnostic Instruments). Colorimetric staining of some sections was performed using Multiple Staining Solution (Polysciences) according to the manufacturer's instructions.

Whole-Mount Staining of Ovaries

Costaining for CYP17A and SHH was performed on whole-mount ovaries from 2-day-old mice. Ovaries were fixed and stored as above, rehydrated into PBS, and permeabilized in PBS-1% Triton X-100. Ovaries were blocked in PBS-0.1% Triton X-100 (PBS-TX) containing 1% BSA and incubated overnight at 4°C with rabbit anti-bovine CYP17A (1:200) and 8 μg/ml goat anti-rabbit SHH (sc-1194; Santa Cruz Biotechnology). Alexa 555-conjugated goat anti-rabbit IgG and Alexa 488-conjugated donkey anti-goat IgG (Invitrogen) were used as second antibodies, and Hoechst 33342 was used for counterstaining. Staining was examined using a Zeiss LSM-510 confocal microscope.

To stain for platelet endothelial cell adhesion molecule (PECAM; also known as PECAM-1 or CD31), whole-mount neonatal ovaries were fixed, stored, rehydrated, and permeabilized as above and then blocked in 5% NGS in PBS-TX. Ovaries were incubated overnight at 4°C with rat anti-mouse PECAM (clone MEC 13.3; BD Pharmingen) diluted 1:25 in PBS-TX-1% BSA, followed by overnight incubation at 4°C with 1 μg/ml Alexa 488-conjugated goat anti-rat IgG (Invitrogen) plus 1 μg/ml Hoechst 33342 in PBS-TX-1% BSA. Using confocal microscopy, a stack of 1-μm-thick images was obtained from the surface of the ovary through the cortex. For each ovary, 15 consecutive images, obtained from 6–20 μm inside the surface of the ovary, were flattened using a z-stack projection (ImageJ software, NIH) and images were processed and analyzed using Photoshop. Staining and imaging were performed in three trials, with each trial including ovaries of representative genotypes and ages. Adjustment of contrast and brightness were constant for ovaries stained in each trial. Green fluorescence (PECAM) was selected using a set color definition, and the area in pixels of PECAM staining was measured and divided by the total area in pixels to determine percentage PECAM staining.

Costaining for PECAM and SMA was used to examine the vasculature of preovulatory follicles. Ovaries were obtained from 24- to 26-day-old mice that had been injected i.p. 48 h earlier with 5 IU equine chorionic gonadotropin (eCG; provided by Dr. A.F. Parlow, National Hormone and Peptide Program, NIDDK) and were fixed and stored as above. Pieces of ovary approximately 150 μm thick and containing numerous preovulatory follicles were cut from the surface of the ovaries, rehydrated, and permeabilized as above and then blocked in 5% NGS in PBS-TX. Tissue was incubated overnight at 4°C with rat anti-mouse PECAM diluted 1:25 in rabbit anti-SMA antibody solution (ab15267; Abcam Inc.; antibody is provided prediluted). This was followed by overnight incubation at 4°C with a second antibody solution consisting of 1 μg/ml Alexa 488-conjugated goat anti-rat IgG, 1 μg/ml Alexa 555-conjugated goat anti-rabbit IgG, and 1 μg/ml Hoechst 33342 in PBS-TX-1% BSA. Tissue was mounted in aqueous mounting media between coverslips using 0.15-μm spacers to preserve depth and examined by confocal microscopy.

Assessment of Oocyte Degeneration and Primordial Follicle Number

Thirty-two serial H&E-stained tissue sections were prepared from ovaries of neonatal mice. Digital images of the cortex at 100× magnification were obtained in every fifth section to generate a total of six regions in which oocytes were counted for each ovary. The morphological criteria used for assessing oocyte degeneration were described previously in detail [14]. The predominant characteristics were nuclear condensation and eosinophilia of the cytoplasm.

Serial sections of ovaries from 24-day-old mice were used to count the number of primordial follicles. Primordial follicles in which the oocyte nucleus was visible were counted in every fourth section at 100× magnification, and the

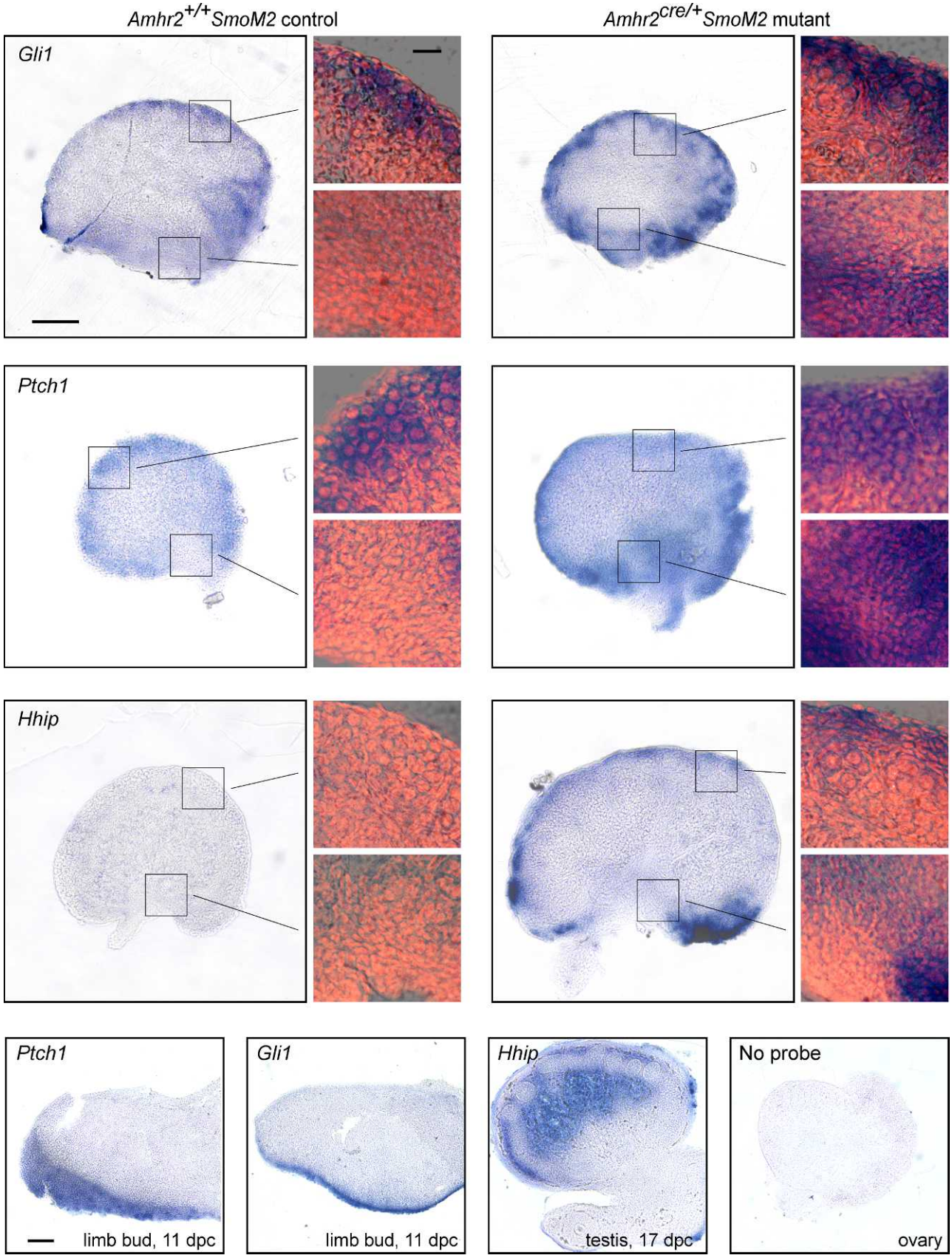

FIG. 3. In situ hybridization for *Gli1*, *Ptch1*, and *Hhip* in ovaries from *Amhr2*$^{+/+}$*SmoM2* control and *Amhr2*$^{cre/+}$*SmoM2* mutant mice on the day of birth. Images are of vibratome sections of whole-mount processed ovaries that are representative of results obtained three to four times for each gene. In high-magnification images, RNA signal (blue) is overlaid over nuclear PI staining (orange). Bottom panels show representative images of limb bud and testis positive control tissues and ovary incubated with no probe as a control for nonspecific signal. Bars = 100 μm (low-magnification images) or 25 μm (high-magnification images).

TABLE 2. Results of DAVID analysis showing clusters of biological process terms associated with genes that were expressed at higher levels in ovaries of *Amhr2*$^{cre/+}$*SmoM2* mutant mice compared to *Amhr2*$^{+/+}$*SmoM2* control mice.[a]

Gene Ontology biological process term[b]	Significance (*P*)
Annotation cluster 1: hormone regulation; enrichment score 6.73	
Hormone metabolic process	5.7×10^{-8}
Cellular hormone metabolic process	2.7×10^{-7}
Regulation of hormone levels	4.1×10^{-7}
Annotation cluster 2: tube development; enrichment score 4.59	
Tube development	4.6×10^{-8}
Epithelium development	3.4×10^{-7}
Morphogenesis of an epithelium	4.2×10^{-7}
Tube morphogenesis	2.0×10^{-6}
Morphogenesis of a branching structure	2.1×10^{-6}
Branching morphogenesis of a tube	5.5×10^{-6}
Tissue morphogenesis	2.2×10^{-5}
Epithelial tube morphogenesis	2.7×10^{-5}
Gland morphogenesis	7.0×10^{-4}
Gland development	7.6×10^{-4}
Urogenital system development	4.4×10^{-3}
Regulation of cell proliferation	3.5×10^{-1}
Annotation cluster 3: respiratory tube development; enrichment score 4.24	
Tube development	4.6×10^{-8}
Respiratory system development	3.5×10^{-4}
Lung development	7.8×10^{-4}
Respiratory tube development	8.8×10^{-4}
Annotation cluster 4: steroid production; enrichment score 3.92	
Steroid biosynthetic process	3.6×10^{-9}
Steroid metabolic process	1.6×10^{-7}
Lipid biosynthetic process	1.3×10^{-5}
Sterol metabolic process	4.1×10^{-4}
Cholesterol metabolic process	1.5×10^{-3}
Isoprenoid metabolic process	1.7×10^{-3}
Sterol biosynthetic process	1.8×10^{-3}
Cholesterol biosynthetic process	7.4×10^{-3}
Isoprenoid biosynthetic process	5.7×10^{-2}
Annotation cluster 5: vascular development; enrichment score 3.25	
Blood vessel development	2.9×10^{-5}
Vasculature development	3.9×10^{-5}
Blood vessel morphogenesis	2.8×10^{-3}
Angiogenesis	3.1×10^{-2}

[a] Genes expressed at least 2-fold higher in mutant ovaries compared to controls, as determined by microarray, were analyzed by DAVID analysis. Only clusters with an enrichment score >3.0 are shown.
[b] Biological process terms are from the Gene Ontology Consortium database.

following formula was used to calculate the total number of primordial follicles in an ovary:

$$\text{No. of follicles} = \text{No. of follicles counted} \times \frac{\text{No. of sections in ovary}}{\text{No. of sections counted}} \times \frac{1}{\text{No. of sections spanned by oocyte nucleus}}$$

The number of sections spanned by the nucleus of an oocyte was determined by dividing the average diameter of the oocyte nucleus in a primordial follicle (12 μm, based on measurement of 12 primordial follicles) by the thickness of the section (5 μm). This formula accounts for the fact that primordial follicles counted in one section would likely be counted in at least one adjacent section.

Quantitative Assessment of Growing Follicles

The percentage of growing follicles that contained more than one oocyte (multiple-oocyte follicles [MOFs]) and the percentage of growing follicles that were atretic were determined in ovaries of 16-day-old mice. Four H&E-stained slides containing eight sections/slide were prepared from an ovary of each mouse. Images at 20× magnification were obtained of every growing follicle in each section (primary follicle or later stage of development) in which the oocyte nucleus was visible. Follicles were classified as atretic or healthy using a weighted scoring system as described previously [15]. Primary characteristics were 1) presence of pycnotic granulosa cells; 2) loss of attachment of granulosa cells to the oocyte or loss of the cumulus cells; 3) presence of leukocytes; and 4) presence of a misshaped, segmented, or discolored oocyte or an oocyte with a condensed nucleus. Secondary characteristics were 1) presence of vacuolated granulosa cells, 2) sparse granulosa cells, and 3) presence of gaps in the basement membrane. Between 100 and 200 follicles from each ovary were scored.

Statistical Analysis

Concentrations of mRNA in whole ovaries, density of cortical capillary network, oocyte degeneration data, and ovarian size data were analyzed by randomized (simple) two-way ANOVA. Concentrations of mRNA were log transformed prior to ANOVA. Student-Newman-Keuls test was used to compare individual means if ANOVA indicated overall significance. All other data were analyzed by unpaired *t*-tests.

RESULTS

Effect of Conditional Expression of SmoM2 in the Ovary on Components of the HH Signaling Pathway

CRE-mediated recombination in ovaries of *Amhr2*$^{cre/+}$*SmoM2* mutant mice was assessed by detection of the SMOM2/YFP fusion protein by confocal microscopy of whole-mount tissue. YFP was detected throughout the ovaries of mutant mice on the day of birth, whereas signal was not detectable in *Amhr2*$^{+/+}$*SmoM2* control ovaries (Fig. 1, panels A–D). These findings are in agreement with previous results using flow cytometry in which 38% of cells from newborn ovaries were positive for YFP [3]. In Day 0 ovaries, it was difficult to distinguish whether YFP was present in oocytes, somatic cells,

TABLE 3. Genes associated with hormone regulation and steroid production that were expressed at higher levels in ovaries of *Amhr2*$^{cre/+}$*SmoM2* mutant mice compared to *Amhr2*$^{+/+}$*SmoM2* control mice.[a]

Gene	Name	Fold[b]	Cluster[c]
Cyp17a1	Cytochrome P450, family 17, subfamily a, polypeptide 1	73.89	H, S
Cyp11a1	Cytochrome P450, family 11, subfamily a, polypeptide 1	61.58	H, S
Adh1	Alcohol dehydrogenase 1 (class I)	39.56	H, S
Star	Steroidogenic acute regulatory protein	13.20	H, S
Shh	Sonic hedgehog	9.25	H, S
Ren1 /// Ren2	Renin 1 structural /// renin 2 tandem duplication of Ren1	7.75	H
Scarb1	Scavenger receptor class B, member 1	4.89	H, S
Hsd3b1	Hydroxy-delta-5-steroid dehydrogenase, 3 beta- and steroid delta-isomerase 1	3.97	S
Sult1e1	Sulfotransferase family 1E, member 1	3.90	H, S
Ddo	D-aspartate oxidase	3.89	H
Fabp3	Fatty acid binding protein 3, muscle and heart	3.66	S
Cyp11b1	Cytochrome P450, family 11, subfamily b, polypeptide 1	3.59	H, S
Idi1	Isopentenyl-diphosphate delta isomerase	3.55	S
Scd1	Stearoyl-Coenzyme A desaturase 1	3.52	S
Fads2	Fatty acid desaturase 2	3.45	S
Sc4mol	Sterol-C4-methyl oxidase-like	3.11	S
Cyp51	Cytochrome P450, family 51	3.05	S
Agt	Angiotensinogen (serpin peptidase inhibitor, clade A, member 8)	2.75	H
Aldh1a3	Aldehyde dehydrogenase family 1, subfamily A3	2.75	H, S
Cyp26b1	Cytochrome P450, family 26, subfamily b, polypeptide 1	2.61	H, S
Cyp21a1	Cytochrome P450, family 21, subfamily a, polypeptide 1	2.40	S
Fads1	Fatty acid desaturase 1	2.35	S
Elovl6	ELOVL family member 6, elongation of long chain fatty acids (yeast)	2.32	S
Tbx3	T-box 3	2.32	H
Hmgcr	3-Hydroxy-3-methylglutaryl-Coenzyme A reductase	2.31	S
Lss	Lanosterol synthase	2.26	S
Ldlr	Low density lipoprotein receptor	2.17	S
Hmgcs1	3-Hydroxy-3-methylglutaryl-Coenzyme A synthase 1 /// similar to Hmgcs1 protein	2.03	S

[a] Levels of mRNA expression were determined by microarray analysis. Biological process terms associated with hormone regulation and steroid production are shown in Table 2; genes listed here have at least one of those terms included in their annotation.
[b] Fold increase in level of expression in mutants compared to controls.
[c] Cluster designation indicates: H, hormone regulation; S, steroid production. Designation with these letters indicates that the gene's annotation includes at least one of the biological process terms associated with the respective cluster. Clusters are shown in Table 2.

or both cell types. However, in ovaries of 10-day-old mice in which oocytes were easily identified in follicles, somatic cells but not oocytes were positive for YFP (Fig. 1, panels E and F).

The expression of genes within the HH pathway was determined during the neonatal period in ovaries of control and mutant mice (Fig. 2). In *Amhr2*$^{+/+}$*SmoM2* control mice, expression of two of the HH ligands, *Dhh* and *Ihh*, increased soon after birth (Day 0). Expression of *Dhh* increased between 17.5 days postcoitum (dpc) and Day 0, continued to increase over time, and remained elevated at Day 16 of age. The pattern of expression of *Ihh* was similar except that expression increased slightly later, by Day 2. The pattern of expression of *Shh* differed from that of *Dhh* and *Ihh* in that it decreased between 17.5 dpc and Day 2 and remained at basal levels until Day 8. In addition, *Shh* expression levels were relatively low, requiring increased numbers of PCR cycles to detect; critical threshold (CT) values for RT-PCR ranged from 35 to 39 for *Shh*, whereas CT values for *Dhh* and *Ihh* ranged from 25 to 31 and from 24 to 33, respectively. Transcription of *Gli1*, *Ptch1*, and *Hhip* are known to increase in response to HH signaling [11, 16–21]. *Gli1* and *Ptch1* increased by Day 2 and *Hhip* increased by Day 4 of age. Expression of *Gli2*, which is a major effector of HH signaling, increased by Day 2 and remained elevated on subsequent days. Thus, transcriptional targets of HH signaling and an effector of HH signaling increased in a pattern consistent with the initial rise in expression of *Dhh* and *Ihh* in the newborn ovary. Expression of *Gli3* and *Smo* remained relatively constant from 17.5 dpc through Day 16.

In ovaries of *Amhr2*$^{cre/+}$*SmoM2* mutant mice, there were no major differences in expression of *Dhh* and *Ihh* compared to controls. In contrast, levels of *Shh* mRNA were elevated in ovaries of mutant mice compared to controls from 17.5 dpc through Day 12. Expression of *Gli1* was higher in ovaries of mutant mice compared to controls between 17.5 dpc and Day 0, and levels of expression of *Ptch1* and *Hhip1* were higher between 17.5 dpc and Day 4. Thus, expression of these HH target genes, which increased in ovaries of control mice between Days 0 and 4 of age, was prematurely elevated in ovaries of mutant mice. Expression of *Gli2* was also elevated in ovaries of mutant mice during the neonatal time period, and this was significant on Day 0. Expression of *Gli3* and *Smo* did not differ in mutants and controls at each time point examined; however, the overall group mean for *Smo* mRNA levels in ovaries of mutant mice across all time points was significantly elevated compared to controls ($P < 0.05$).

In situ hybridization of ovaries of control and mutant mice on Day 0 (Fig. 3) showed that *Gli1* and *Ptch1* were expressed in the cortex in areas containing cords. Ovaries of mutant mice showed additional areas of *Gli1* and *Ptch1* expression in the medulla, close to the hilar region, that were not observed in control ovaries. *Hhip* expression was not detectable in ovaries of control mice but was observed in the cortex and medulla of ovaries of mutant mice. Taken together, the results show that elevated expression of *Gli1*, *Ptch1*, and *Hhip* in ovaries of mutant mice compared to control mice detected by RT-PCR (Fig. 2) appears to be due to regions of expression in the medulla in mutant ovaries that are absent in controls. Controls for the in situ hybridization procedure showed the expected signals for *Ptch1* and *Gli1* in the posterior region of the mouse limb bud on 11 dpc [22] and for *Hhip* in 17 dpc testis [11], and lack of signal in the absence of probe (Fig. 3).

TABLE 4. Genes associated with tube development and vascular development that were expressed at higher levels in ovaries of *Amhr2*$^{cre/+}$*SmoM2* mutant mice compared to *Amhr2*$^{+/+}$*SmoM2* control mice.[a]

Gene	Name	Fold[b]	Cluster[c]
Hhip	Hedgehog-interacting protein	50.38	T
Shh	Sonic hedgehog	9.25	T, V
Ren1 /// Ren2	Renin 1 structural /// renin 2 tandem duplication of Ren1	7.75	T
Foxf1a	Forkhead box F1a	6.02	T, V
Hk2	Hexokinase 2	5.30	T
Enpep	Glutamyl aminopeptidase	4.93	V
Prlr	Prolactin receptor	4.57	T
Crispld2	Cysteine-rich secretory protein LCCL domain containing 2	4.03	T
Tbx18	T-box18	3.70	T
Figf	C-fos induced growth factor	3.58	T, V
Ntrk2	Neurotrophic tyrosine kinase, receptor, type 2	3.08	V
Angpt2	Angiopoietin 2	2.97	V
Ptch1	Patched homolog 1	2.84	T
Agt	Angiotensinogen (serpin peptidase inhibitor, clade A, member 8)	2.75	T, V
Aldh1a3	Aldehyde dehydrogenase family 1, subfamily A3	2.75	T
Nrp1	Neuropilin 1	2.68	T, V
Ntn1	Similar to Netrin-1 precursor /// netrin 1	2.49	T
Osr2	Odd-skipped related 2 (*Drosophila*)	2.48	T
Ccl11	Chemokine (C-C motif) ligand 11	2.48	T
Cxcr4	Chemokine (C-X-C motif) receptor 4	2.47	T,V
Mef2c	Myocyte enhancer factor 2C	2.47	V
Lox	Lysyl oxidase	2.44	T,V
Adm	Adrenomedullin	2.39	T
Gdnf	Glial cell line derived neurotrophic factor	2.34	T
Ppap2b	Phosphatidic acid phosphatase type 2B	2.33	V
Tbx3	T-box 3	2.32	T,V
Fzd2	Frizzled homolog 2 (*Drosophila*)	2.30	T
Gja1	Gap junction protein, alpha 1	2.27	T,V
Zeb2	Zinc finger E-box binding homeobox 2	2.24	T
Igf1	Insulin-like growth factor 1	2.23	T
Pdgfra	Platelet derived growth factor receptor, alpha polypeptide	2.19	T
Sfrp1	Secreted frizzled-related protein 1	2.17	T
Ctgf	Connective tissue growth factor	2.15	T,V
Lipa	Lysosomal acid lipase A	2.15	T
Wnt5a	Wingless-related MMTV integration site 5A	2.14	T
Gpc3	Glypican 3	2.09	T
Col1a1	Collagen, type I, alpha 1	2.08	V
Hoxa9	Homeo box A9	2.02	T

[a] Levels of mRNA expression were determined by microarray analysis. Biological process terms associated with tube development and vascular development are shown in Table 2; genes listed here have at least one of those terms included in their annotation.
[b] Fold increase in level of expression in mutants compared to controls.
[c] Cluster designation indicates: T, tube development; V, vascular development. Designation with these letters indicates that the gene's annotation includes at least one of the biological process terms associated with the respective cluster. Clusters are shown in Table 2.

Microarray Analysis

Microarray analysis of gene expression was performed on RNA prepared from ovaries of *Amhr2*$^{cre/+}$*SmoM2* mutant and control mice on Day 2 of age in order to obtain insight into pathways altered by dominant activation of HH signaling (microarray data, accession No. GSE35123, are available at http://www.ncbi.nlm.nih.gov/geo/query/acc.cgi?acc=GSE35123). There were 416 transcripts representing 345 genes that were expressed at least 2-fold higher in mutants compared to controls (Supplemental Table S1; all Supplemental Data are available online at www.biolreprod.org) and 189 transcripts representing 180 genes that were expressed at least 2-fold lower in mutants compared to controls (Supplemental Table S2). DAVID cluster analysis [23, 24] of biological process terms from the Gene Ontology Consortium was used to identify related groups of biological process terms that were overrepresented (enriched) among the genes that were 2-fold higher in mutants compared to controls. Five highly enriched clusters of terms, with enrichment scores >3.0, were identified (Table 2). The five clusters were designated by the authors as hormone regulation, tube development, respiratory tube development, steroid production, and vascular development. Examination of the genes that were expressed 2-fold higher in mutants and whose annotations included the biological process terms within the five clusters showed that hormone regulation and steroid production were closely related; 10 of the 14 genes associated with hormone regulation were also associated with steroid production (Table 3). Similarly, tube development, respiratory tube development, and vascular development clusters were closely related. All of the 21 genes associated with respiratory tube development were also associated with tube development (denoted by T in Table 4), and 10 of the 16 genes associated with vascular development were also associated with tube development.

When DAVID analysis was applied to genes that were 2-fold lower in mutants, a single cluster of terms had an enrichment score >3.0; this cluster was termed gamete development by the authors. Biological process terms associated with this gamete development cluster are shown in Supplemental Table S3, and genes with these terms in their annotations that were expressed 2-fold lower in mutants compared to controls are shown in Supplemental Table S4.

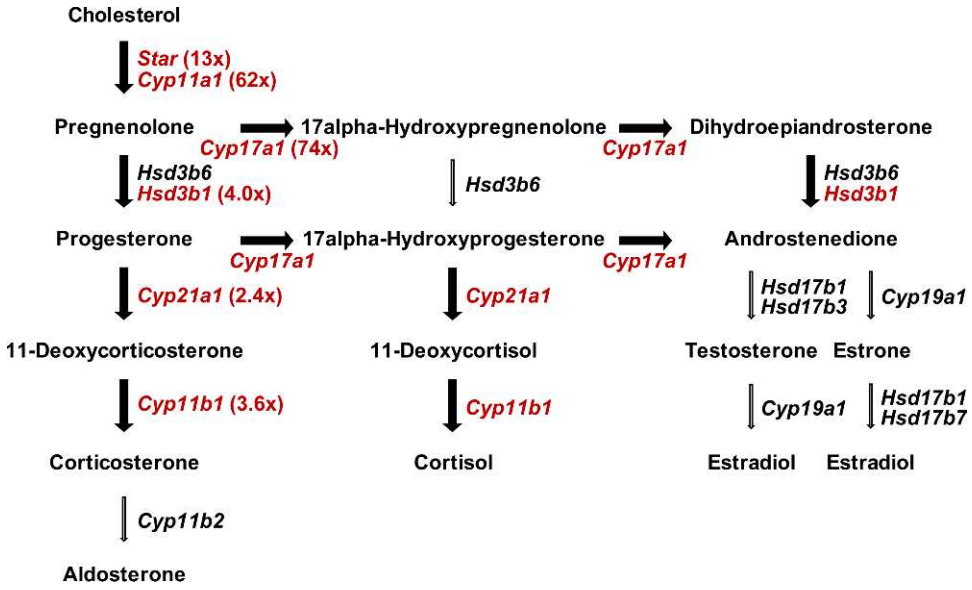

FIG. 4. Genes encoding key enzymes in the steroidogenic pathways in the gonads and adrenal gland. Levels of mRNA for genes highlighted in red are elevated in whole ovaries of mutant mice compared to controls based on the results of microarray analysis (shown in Table 3). The fold increases in expression in mutants compared to controls are indicated in parentheses.

Steroidogenic Enzymes in Ovaries of Control and Mutant Mice

Microarray data indicated negligible expression of several genes for steroidogenic enzymes in ovaries of control mice, as would be expected on Day 2 of age. In contrast, comparatively higher levels of these genes were expressed in ovaries of mutant mice, as shown diagrammatically in Figure 4, and suggest the potential for production of androgens and corticosterone. Real time RT-PCR showed that in ovaries of control mice, *Star* was expressed at low levels from 17.5 dpc through Day 4, increased on Day 8, and continued to rise on Days 12 and 16, consistent with steroid production by the first wave of growing follicles (Fig. 5A). In ovaries of mutant mice, *Star* mRNA levels were significantly elevated from 17.5 dpc through Day 8 and then became similar to levels in control ovaries on Days 12 and 16 (Fig. 5A). CYP17A, an enzyme required for androgen production, was not detectable by immunohistochemistry in control ovaries between 17.5 dpc and Day 16. In contrast, CYP17A-positive cells were present in the medulla of ovaries from mutant mice; although staining was detectable in ovaries on 17.5 dpc through Day 16, it was most prominent on Days 0 and 2 (Fig. 5B). Staining for CYP21A, the enzyme required for production of corticosterone, was present in the medulla in many of the same cells positive for CYP17A on Day 0 (Fig. 5C).

SHH is known to be expressed in the developing adrenal and to influence the fate of steroidogenic adrenal cells [1, 25]. Immunohistochemistry for SHH revealed a small number of SHH-positive cells in the medulla of ovaries of mutant mice in the same vicinity as cells positive for CYP17A (Fig. 5C).

Increased Density of Capillaries in the Ovarian Cortex of Mutant Mice

The enrichment for genes involved in vascular development/tube formation in ovaries of mutant mice, suggested by microarray analysis, was further investigated by staining for the endothelial cell marker PECAM. The capillary network observed in stacks of confocal images was denser in the cortex region of ovaries of mutant mice compared to controls (Fig. 6A) and quantification showed that the area of the cortex occupied by PECAM-positive staining was significantly elevated on Days 2 and 4 (Fig. 6B).

Deficient Vascular Smooth Muscle in Theca of Mutant Mice

Our previous work showed that anovulation in *Amhr2*$^{cre/+}$*SmoM2* mutant mice is associated with a deficit of staining for the muscle marker SMA in the theca of growing and preovulatory follicles [3]. In order to test whether the cells altered in the theca of mutant mice represent muscle-type mural support cells (pericytes and vascular smooth muscle cells), whole-mount preparations of ovaries of eCG-primed immature mice were costained for SMA and PECAM, and confocal microscopy was used to visualize successive 6-μm stacks through the walls of preovulatory follicles as diagrammed in Fig. 7A. Imaging through the outermost region of the follicle wall in control mice showed extensive association of SMA-positive cells with large PECAM-labeled vessels (Fig. 7B, upper panels, arrowheads). Imaging of progressively deeper stacks through the walls of follicles in control mice showed small PECAM-labeled vessels that were also associated with SMA-positive cells and an innermost plexus of endothelial tubes that had only sparse staining with SMA (Fig. 7B, upper panels, arrows). PECAM staining in layers through the theca of mutant mice was similar to that observed in control mice; however, there was a severe reduction in SMA labeling (Fig. 7B, lower panels).

Alteration of Early Follicle Development in Mutant Mice

Cord breakdown and follicle formation are associated with a high frequency of oocyte death [6, 14]. Consistent with this, the percentages of oocytes that were clearly condensed and undergoing degeneration were substantial from 17.5 dpc through Day 4 in *Amhr2*$^{+/+}$*SmoM2* control mice (Fig. 8, A and B). At 17.5 dpc, the percentage of oocytes that were degenerating was higher in ovaries of control mice than in

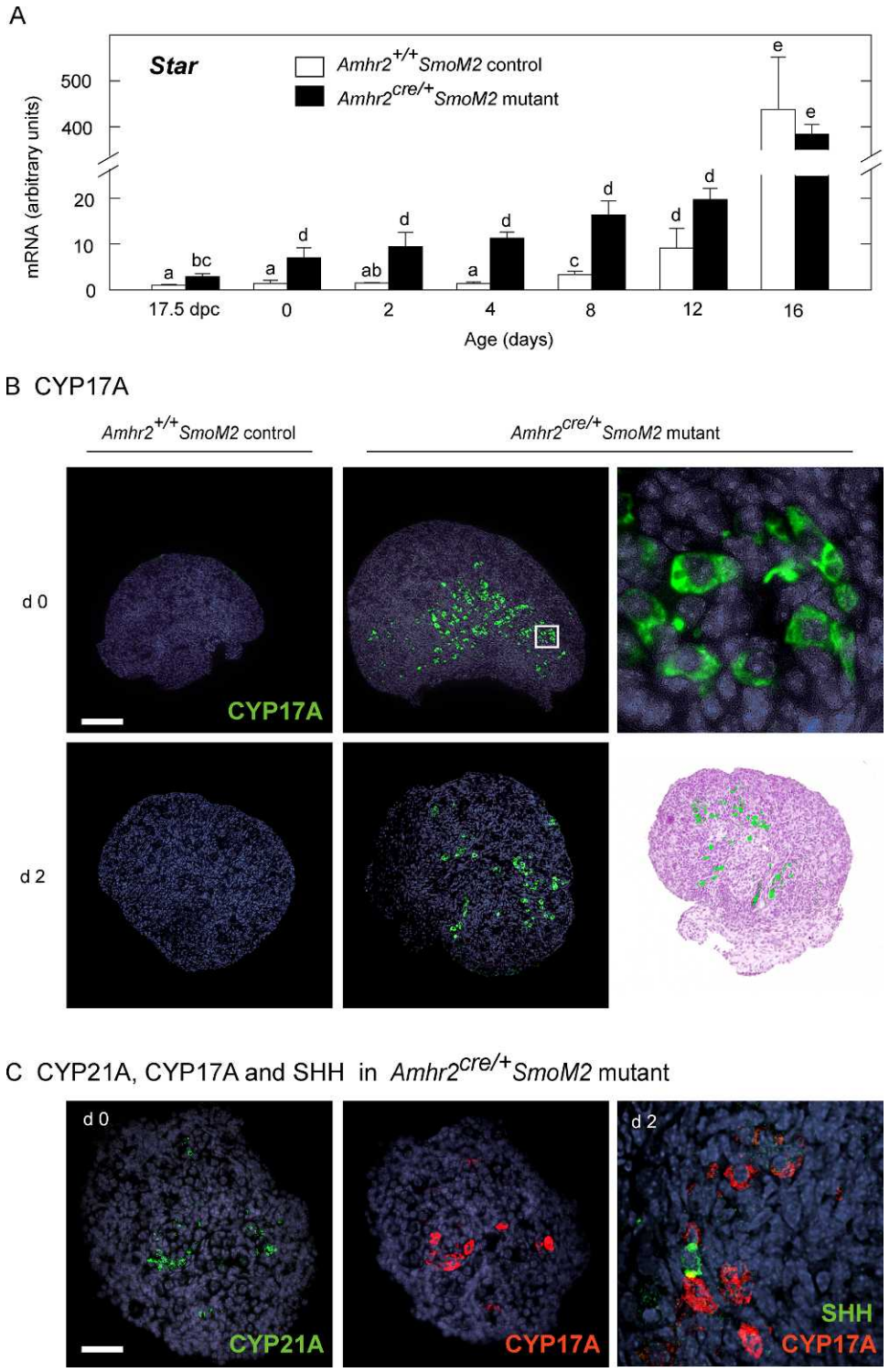

FIG. 5. Expression of *Star,* CYP17A, CYP21A, and SHH in *Amhr2*$^{+/+}$*SmoM2* control and *Amhr2*$^{cre/+}$*SmoM2* mutant mice. **A**) Real-time RT-PCR for *Star* in whole ovaries was carried out as described in the legend to Figure 2. Data are mean ± SEM (n = 3 RNA preparations). Bars without common superscripts are significantly different ($P < 0.05$). **B**) Immunofluorescence for CYP17A in sections of ovaries of control and mutant mice at 0 and 2 days of age counterstained with Hoechst 33342 (blue) to show nuclei. The framed area in the Day 0 ovary is enlarged as the image to the right. Stainings of CYP17A and Multiple Staining Solution were performed on adjacent sections of a Day 2 mutant mouse ovary and images overlaid to show the localization of CYP17A-positive cells. All images are oriented with the medulla at the bottom. Bar = 6 μm for the enlarged image and 100 μm for all other images. Images are representative of results obtained using more than 4 mice of each genotype and age. **C**) Immunofluorescence for CYP21A and CYP17A in adjacent sections of the same ovary on Day 0 and costaining for SHH and CYP17A in a whole-mount ovary on Day 2. Bar = 50 μm for CYP21A and CYP17A and 15 μm for SHH/CYP17A costaining.

mutant mice. From Day 0 through Day 4, however, the percentage of degenerating oocytes was numerically higher in ovaries of mutant mice, and this difference was significant on Day 0 (Fig. 8B). Cord breakdown and the associated formation of primordial follicles occurred with similar timing in mutants and controls and were complete by Day 4. Counts of primordial follicles in serial sections of 24-day-old mice indicated that there were 25% fewer primordial follicles in ovaries of mutant mice compared to controls (Fig. 8C).

Ovaries of mutant mice were consistently larger than ovaries of control mice. Histological sections from ovaries on Days 0 and 2 showed that the medulla of mutant ovaries was expanded compared to that in control ovaries (Fig. 9A). Visible surface area, calculated from images of ovaries, was increased in mutant ovaries compared to controls on Days 0–4 (Fig. 9B).

During the first wave of follicle growth, secondary and tertiary follicles with two or more layers of granulosa cells were observed as expected in the ovaries of control mice (Fig. 10A). In ovaries of mutant mice, a large proportion of follicles with two layers of granulosa cells had an abnormal gap between cell layers (Fig. 10A), and there was a higher percentage of atretic follicles than in control mice (Fig. 10B). MOFs were present at a higher frequency in ovaries of mutant mice compared to controls (Fig. 10, A and B). By 24 days of age, there were no obvious differences in the histological appearance of follicles in mutant and control mice (Fig. 10A).

DISCUSSION

Low-level activation of HH signaling in the ovaries of control mice during the first few days of life, as indicated by expression of the transcriptional targets of HH signaling, *Gli1*, *Ptch1*, and *Hhip*, is consistent with expression of HH pathway genes in early growing follicles, as shown in previous studies [8]. Primary follicles were observed as early as Day 0 in both mutants and controls and increased in number on Days 2 and 4. The prominent increase in HH activity observed between Days 4 and 8 corresponds to the time period when follicles within the first wave of growing primary follicles reach the secondary stage. In ovaries of mutant mice, levels of mRNA for *Gli1*, *Ptch1*, and *Hhip* were elevated during the first few days of life compared to controls, and in situ hybridization of ovaries isolated on the day of birth showed that expression of these genes was elevated in a region of the medulla near the hilus. The SMOM2/YFP fusion protein was expressed in cells throughout the newborn ovary of *Amhr2*$^{cre/+}$*SmoM2* mice, consistent with the original report that CRE-mediated recombination through the *Amhr2*$^{cre/+}$ allele occurs in somatic cells of the gonad beginning at 12.5 dpc [10]. Studies have indicated that cell types differ in their response to expression of SMOM2/YFP; whereas some cell types had increased expression of the downstream target genes *Gli1* and *Ptch1*, others failed to show this response, suggesting that they lacked the capability to respond to HH signaling [26, 27]. In the current study, cells capable of responding to SMOM2 with increased HH pathway activity resided in the hilar region of the ovary.

By Day 8 of age, when the first wave of follicle growth was underway, expression of *Gli1*, *Ptch1*, and *Hhip* no longer differed in ovaries of *Amhr2*$^{cre/+}$*SmoM2* mutant and control mice. This normalization of HH target gene expression is consistent with our previous report using prepubertal *Amhr2*$^{cre/+}$*SmoM2* mice, in which levels of mRNA for HH pathway genes did not differ in gonadotropin-stimulated preovulatory follicles of mutants and controls (including *Gli1, Ptch1*, *Hhip*, *Ihh*, and *Gli3*) [3]. Despite the apparent

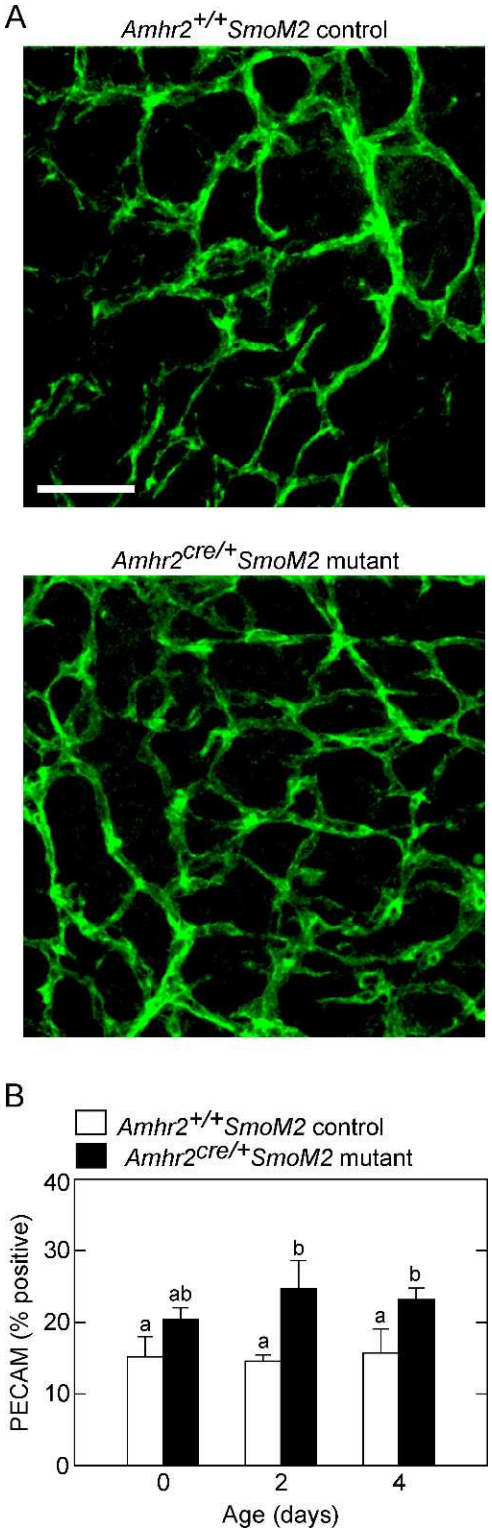

FIG. 6. Density of capillaries in the ovarian cortex of *Amhr2*$^{+/+}$*SmoM2* control and *Amhr2*$^{cre/+}$*SmoM2* mutant mice. **A**) Representative projections of staining of whole-mount ovaries from 2-day-old mice. Projections represent 15 consecutive 1-μm-thick images obtained from the cortex of the ovary. Bar = 50 μm. **B**) Quantification of the percentage of total area stained positively for PECAM. Data represent the mean ± SEM (n = 3 mice). Bars without common superscripts are significantly different ($P < 0.05$).

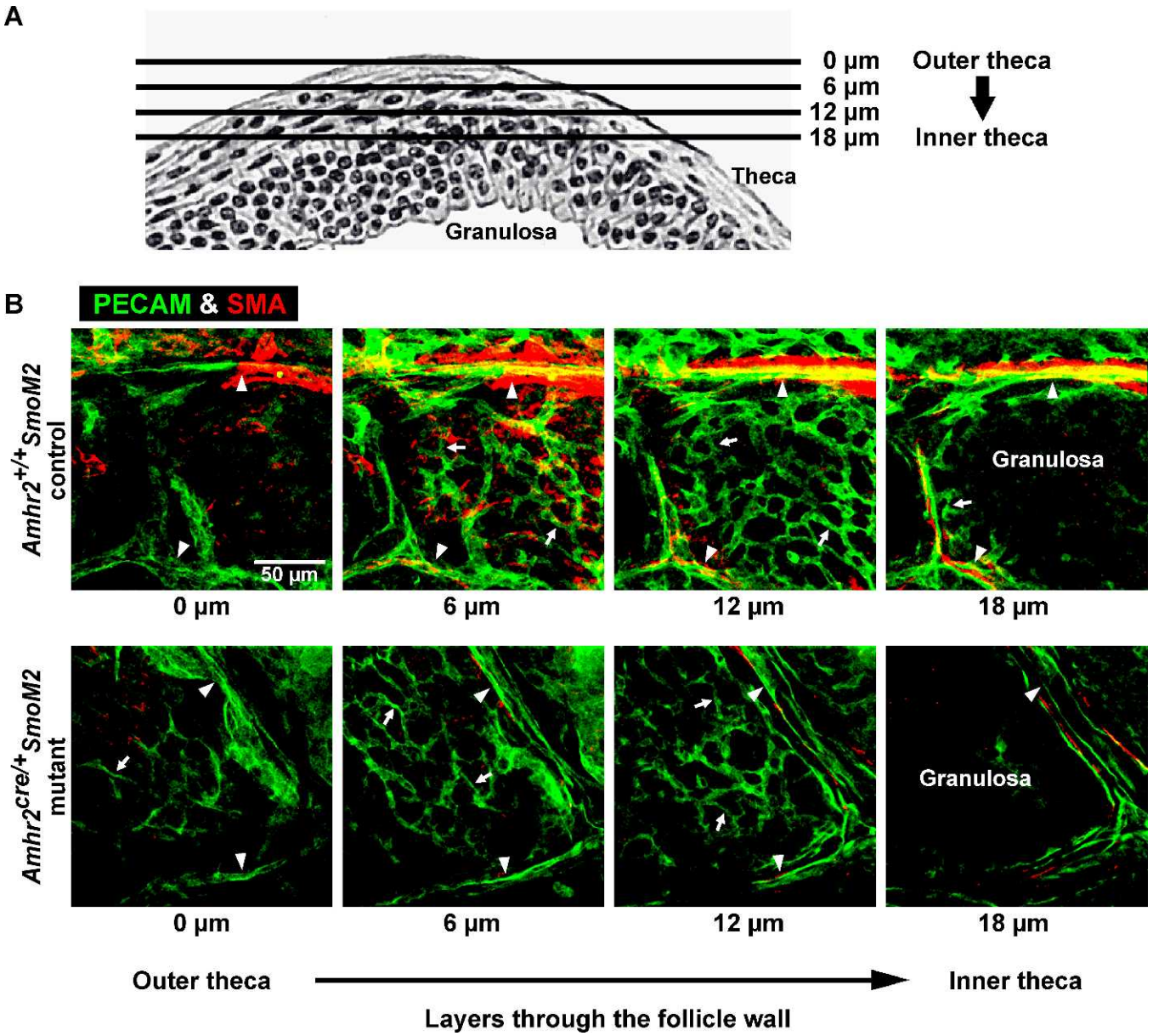

FIG. 7. Confocal imaging of preovulatory follicles costained for PECAM (green) and SMA (red) in whole-mount preparations of ovaries from eCG-primed prepubertal mice. Successive 6-μm stacks through the walls of individual preovulatory follicles were imaged, as diagrammed in **A**, and representative series of images are shown in **B**. Arrowheads point to large vessels within the theca that are visible in multiple successive layers through the follicle wall of the control and mutant. In the control follicle, these large vessels are associated with SMA-stained cells, whereas in the mutant follicle SMA staining is minimal. Arrows point to small vessels that are similarly visible at multiple layers of the follicles in control and mutant mice but that are associated only with SMA-positive cells in controls.

normalization of HH pathway activity, the physiological function of the ovary in mutant mice was dramatically altered; whereas preovulatory follicles developed in mutant mice and underwent many of the expected changes in gene expression and morphology after eCG/hCG treatment, follicle rupture failed to occur and corpora lutea formed around trapped oocytes. This phenotype was associated with reduced ovarian expression of genes typical of smooth muscle as well as dramatically reduced staining for SMA in the theca layer of growing and preovulatory follicles [3]. In the current study, costaining for the endothelial cell marker, PECAM, and SMA in ovaries of eCG-primed mice and examination of successive layers through preovulatory follicles using confocal microscopy showed that blood vessels within the theca of mutant mice are deficient in vascular smooth muscle.

Potential effects of HH signaling on the ovarian vasculature are supported by microarray data that showed that genes expressed at higher levels in ovaries of 2-day-old *Amhr2*$^{cre/+}$*SmoM2* mutant mice compared to controls were enriched for genes involved in vascular and tube development. In addition, the density of PECAM-positive endothelial cells in the cortex of ovaries from mutant mice was increased relative to controls on Days 2 and 4. HH signaling is known to regulate multiple aspects of vascular development, including vasculogenesis, which is the formation of endothelial cell tubes directly from mesodermal precursors, and angiogenesis, which is the extension or remodeling of existing vessels by outgrowth of vascular sprouts [28–32]. Furthermore, HH signaling influences the fate of vessels to become arterioles or veins [33] and regulates the maturation process whereby vessels become associated with mural support cells (vascular smooth

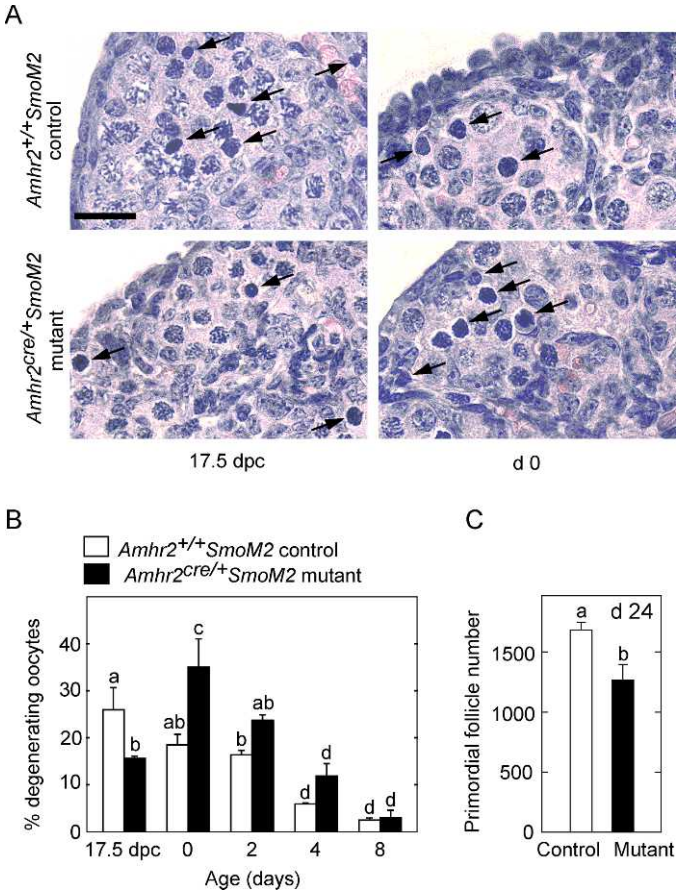

FIG. 8. Quantification of degenerating oocytes and the number of primordial follicles in ovaries of *Amhr2*$^{+/+}$*SmoM2* control and *Amhr2*$^{cre/+}$*SmoM2* mutant mice. **A**) Representative fields of H&E-stained sections of ovaries from control and mutant mice on 17.5 dpc and Day 0. Arrows point to examples of degenerating oocytes. Bar = 20 μm. **B**) Quantification of the percentage of degenerating oocytes in the cortex. **C**) Numbers of primordial follicles counted in serial sections of ovaries from 24-day-old mice. Data in **B** and **C** represent the mean ± SEM (n = 3 mice). Bars without common superscripts are significantly different ($P < 0.05$).

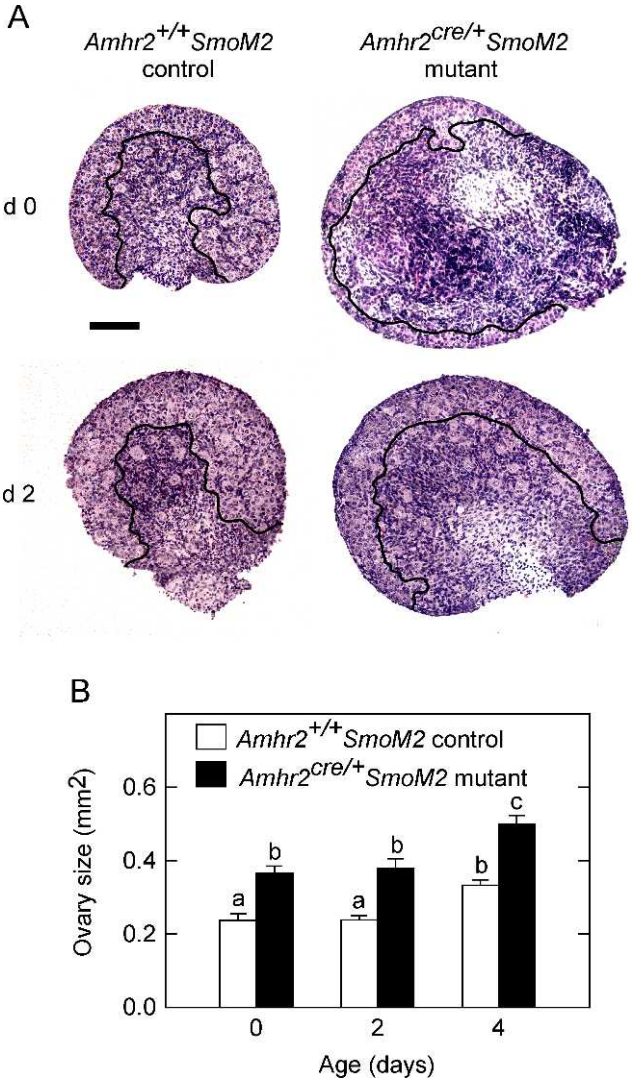

FIG. 9. Size differences in ovaries of *Amhr2*$^{+/+}$*SmoM2* control and *Amhr2*$^{cre/+}$*SmoM2* mutant mice during folliculogenesis. **A**) The representative H&E-stained sections shown are through the largest cross section of ovaries on Days 0 and 2. Black lines delineate the boundary between the cortex and medulla regions of the ovary. Bar = 100 μm. **B**) Area of ovary, obtained from images of fresh, unfixed ovaries. Data are mean ± SEM of measurements obtained from at least 4 mice on each day. Bars without common superscripts are significantly different ($P < 0.05$).

muscle and pericytes), frequently by direct actions on vascular mural cells or mesenchymal cells [34–37]. It is therefore possible that HH signaling regulates vascular development in follicles. Additional work is required to determine in detail the link between overactivation of HH signaling in the ovaries of neonatal *Amhr2*$^{cre/+}$*SmoM2* mice and failure of vessels in the developing theca of individual follicles to become properly associated with vascular smooth muscle throughout life. Possibilities include long-term effects on 1) the number of vascular smooth muscle precursors; 2) signals that direct differentiation of precursors into vascular smooth muscle cells and/or recruit them to blood vessels; or 3) expression of inhibitors of vascular maturation.

Another alteration in ovaries of *Amhr2*$^{cre/+}$*SmoM2* mutant mice observed by microarray analysis was expression of genes typical of adrenal corticoid-producing cells, including *Cyp21a* and *Cyp11b1*. Expression of *Cyp17a*, which is required for androgen production [38], was also increased in mutant ovaries and is known to be expressed during development of the embryonic mouse adrenal [38, 39]. Immunohistochemistry revealed cells positive for both CYP17A and CYP21A in the medulla of *Amhr2*$^{cre/+}$*SmoM2* mutant ovaries, but not control ovaries, on Day 0 through Day 8, and *Star* mRNA was elevated from 17.5 dpc through Day 8. A potential explanation for this altered gene expression is that adrenal and gonadal cells share a common embryonic precursor known as the adrenal-gonadal primordium and that missorting of adrenal precursor cells during development can lead to their presence in the gonads [1]. Testicular masses, known as adrenal rest tissue, are thought to be derived from ectopic adrenal tissue that has failed to separate from the gonad during fetal differentiation [40, 41]. Female mice null for *Wnt4* have ectopic adrenal precursor cells in the medulla of the ovary that arise by migration from the adrenal primordium [39, 42, 43] and express genes typical of adrenal cells (*Cyp11b2* and *Cyp21a*) and genes required for androgen production (*Cyp17a*, *Hsd17b1,* and *Hsd17b3*) [39, 42, 44]. Excess production of androgen during embryonic development in ovaries of *Wnt4* null mice leads to partial sex reversal [44]. Although ovaries of *Amhr2*$^{cre/+}$*SmoM2* mutant mice express *Cyp17a* mRNA and CYP17A protein, and could therefore potentially produce DHEA and androstenedione, microarrays show that mutant and control mice have

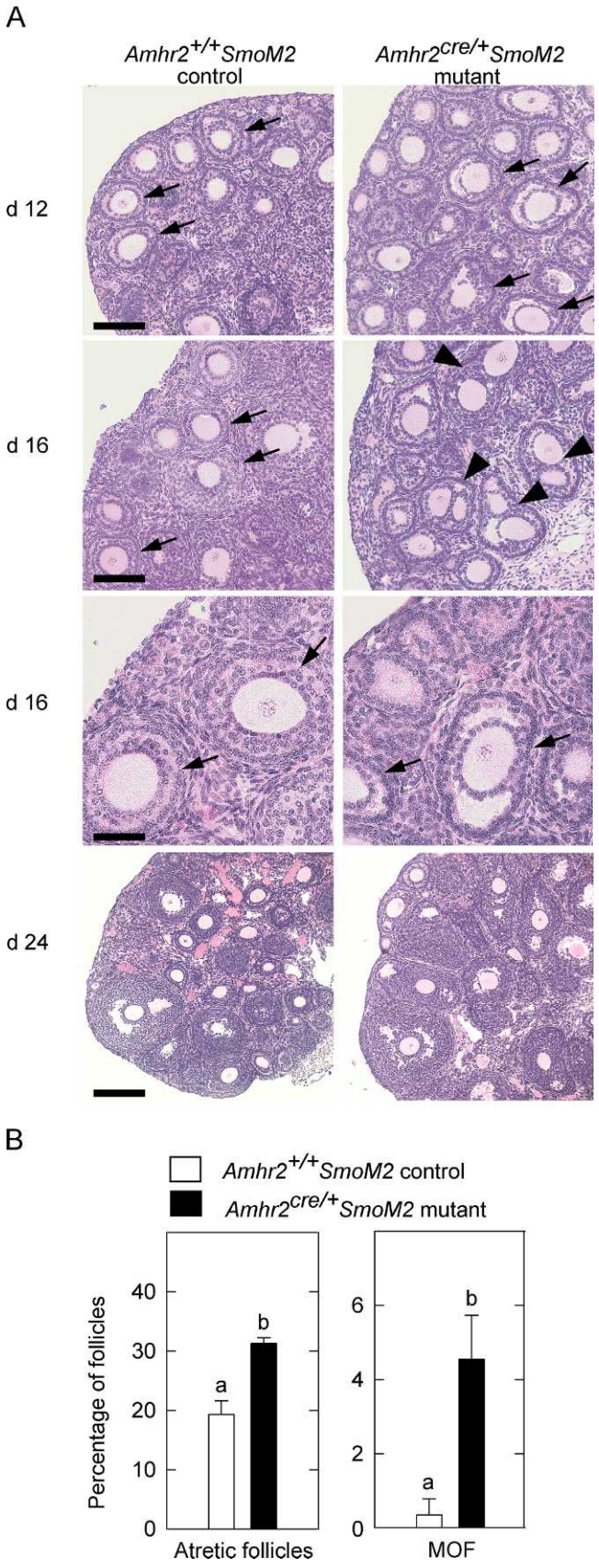

FIG. 10. Morphology of follicles during the first wave of follicle development in *Amhr2*$^{+/+}$*SmoM2* control and *Amhr2*$^{cre/+}$*SmoM2* mutant mice. **A**) Representative H&E-stained sections of ovaries from control and mutant mice. Arrows point to examples of follicles with two or more layers of granulosa cells; in mutants, these follicles have an abnormal gap between layers of granulosa cells. Arrowheads point to examples of MOFs in *Amhr2*$^{cre/+}$*SmoM2* mutant mice. Bar = 100 μm for Day 12 and Day 16 ovaries, 50 μm for the enlarged images of Day 16 ovaries, and 200 μm for Day 24 ovaries. **B**) Quantification of atretic follicles and MOFs as a percentage of growing follicles in sections of ovaries on Day 16. Data are mean ± SEM (n = 3 mice). Bars without common superscripts are significantly different ($P < 0.05$).

undetectable levels of *Hsd17b3*, which is required for production of testosterone. *Amhr2*$^{cre/+}$*SmoM2* female mice have normal regression of the Wolffian duct and no obvious signs of masculinization [45], suggesting that androgen production is not sufficient and/or occurs too late in development to cause sex reversal.

The fact that levels of expression of *Shh* were elevated between 17.5 dpc and Day 12 in mutant mice compared to barely detectable levels in controls and the finding of a small number of SHH-positive cells in the medulla of mutant ovaries may be due to the presence of adrenal-type cells. In the embryonic adrenal, SHH-expressing cells in the subcapsular cortex regulate cell differentiation and expression of genes for steroidogenic enzymes [1, 25]. *Smoc2*, another gene shown by microarrays to be elevated in ovaries of *Amhr2*$^{cre/+}$*SmoM2* mice compared to controls (5.7-fold higher), and that is increased in response to HH signaling [46], is normally expressed in the embryonic adrenal cortex and was expressed by ectopic steroidogenic cells in the ovaries of *Wnt4* null mice [46]. It is therefore possible that elevated expression of *Shh* and *Smoc2* in ovaries of *Amhr2*$^{cre/+}$*SmoM2* mice during early life is due to the presence of adrenal-type cells.

In a previous study, mice were created in which *SmoM2* was conditionally expressed in the ovary by CRE-mediated recombination using the SF1-cre allele [47]. Ovaries of SF1/Cre; Smo^{YFP} mice contained cells that expressed CYP17A and that were postulated to represent Leydig cells that had differentiated under the influence of HH signaling; these cells were postulated to produce androgen based on the fact that females developed as pseudohermaphrodites in which the Wolffian ducts were maintained and the ovaries adopted a descended position in the abdominal cavity. Whether the CYP17A-producing cells within the ovaries may have also had properties of adrenal cells was not reported [47].

Aspects of early follicle development were abnormal in *Amhr2*$^{cre/+}$*SmoM2* mutant mice. On Day 0, the percentage of degenerating oocytes was elevated in mutant mice, and on Day 24, the number of primordial follicles was reduced, suggesting reduced oocyte survival. In addition, multiple oocytes were observed within single follicles, indicating that cord breakdown and follicle formation were moderately affected. Secondary follicles with an abnormal gap between layers of granulosa cells were observed in ovaries of mutant mice only early in life, suggesting that the first wave of follicle development was most affected. Because vascularization is critical for cord formation in the testis [48] and provides developmental signals during pancreas and liver organogenesis [49, 50], it is possible that changes in vascularization of ovaries in *Amhr2*$^{cre/+}$*SmoM2* mutant mice may alter development. Alteration in the first wave of follicle development in mutant mice may also be related to the abnormal production of steroids in the medulla. The cause of the increased area of the medulla in mutant mice compared to controls is not known, although increased numbers of vascular cells and the presence of adrenal-type cells may potentially contribute.

In summary, HH signaling is active in the neonatal ovary when the first follicles begin to grow. In *Amhr2*$^{cre/+}$*SmoM2*

mutant mice, overactivation of HH signaling occurred during embryonic development and through the first several days of life, but activity normalized thereafter. This early overactivation of HH signaling modified ovarian vascular development and caused steroidogenic cells with properties of adrenal cells to appear in the neonatal ovary. The findings suggest that the lifelong anovulatory phenotype in *Amhr2*$^{cre/+}$*SmoM2* mice and the associated deficit in vascular smooth muscle in the theca may be caused by developmental disturbances occurring primarily during the embryonic/neonatal period. These results have implications for human disorders in which HH signaling is overactivated. For example, Gorlin syndrome, which is caused by mutations in PTCH1 that result in overactivation of HH signaling, is associated with a high frequency of development of ovarian fibromas [51–54]. Further research on the role of HH signaling in the regulation of follicular vascular development is warranted.

ACKNOWLEDGMENT

The authors thank Richard R. Behringer, University of Texas M.D. Anderson Cancer Center, Houston, Texas, for providing *Amhr2*$^{cre/+}$ mice; Andrew P. McMahon, Harvard University, for the *Hhip* probe; Alexandra L. Joyner, Memorial Sloan-Kettering Cancer Center, for the *Gli1* probe; and Timothy P. O'Brien, New York State College of Veterinary Medicine, Cornell University, for the *Ptch1* probe. Ian C. Welsh, Cornell University College of Veterinary Medicine, was invaluable in assisting us with in situ hybridization. We also thank Alan J. Conley, University of California at Davis, for the CYP17A antibody and Walter L. Miller, University of California at San Francisco, for the CYP21A antibody.

REFERENCES

1. King PJ, Guasti L, Laufer E. Hedgehog signalling in endocrine development and disease. J Endocrinol 2008; 198:439–450.
2. Huangfu D, Anderson KV. Signaling from Smo to Ci/Gli: conservation and divergence of Hedgehog pathways from *Drosophila* to vertebrates. Development 2006; 133:3–14.
3. Ren Y, Cowan RG, Harman RM, Quirk SM. Dominant activation of the hedgehog signaling pathway in the ovary alters theca development and prevents ovulation. Mol Endocrinol 2009; 23:711–723.
4. Xie J, Murone M, Luoh SM, Ryan A, Gu Q, Zhang C, Bonifas JM, Lam CW, Hynes M, Goddard A, Rosenthal A, Epstein EH Jr, et al. Activating Smoothened mutations in sporadic basal-cell carcinoma. Nature 1998; 391:90–92.
5. Jeong J, Mao J, Tenzen T, Kottmann AH, McMahon AP. Hedgehog signaling in the neural crest cells regulates the patterning and growth of facial primordia. Genes Dev 2004; 18:937–951.
6. Pepling ME. From primordial germ cell to primordial follicle: mammalian female germ cell development. Genesis 2006; 44:622–632.
7. Mazaud S, Guyot R, Guigon CJ, Coudouel N, Le Magueresse-Battistoni B, Magre S. Basal membrane remodeling during follicle histogenesis in the rat ovary: contribution of proteinases of the MMP and PA families. Dev Biol 2004; 277:403–416.
8. Wijgerde M, Ooms M, Hoogerbrugge JW, Grootegoed JA. Hedgehog signaling in mouse ovary: Indian hedgehog and desert hedgehog induce target gene expression in developing theca cells. Endocrinology 2005; 146:3558–3566.
9. Russell MC, Cowan RG, Harman RM, Walker AL, Quirk SM. The hedgehog signaling pathway in the mouse ovary. Biol Reprod 2007; 77: 226–236.
10. Jamin SP, Arango NA, Mishina Y, Hanks MC, Behringer RR. Requirement of Bmpr1a for Mullerian duct regression during male sexual development. Nat Genet 2002; 32:408–410.
11. Chuang P, McMahon AP. Vertebrate Hedgehog signalling modulated by induction of a Hedgehog-binding protein. Nature 1999; 397:617–621.
12. Corrales JD, Rocco GL, Blaess S, Guo S, Joyner AL. Spatial pattern of sonic hedgehog signaling through Gli genes during cerebellum development. Development 2004; 131:5581–5590.
13. Welsh IC, Hagge-Greenberg A, O'Brien TP. A dosage-dependent role for Spry2 in growth and patterning during palate development. Mech Dev 2007; 124:746–761.
14. Beaumont HM, Mandl AM. A quantitative and cytological study of oogonia and oocytes in the foetal and neonetal rat. Proc R Soc Lond 1962; 155:557–579.
15. Boyer A, Lapointe E, Zheng X, Cowan RG, Li H, Quirk SM, DeMayo FJ, Richards JS, Boerboom D. WNT4 is required for normal ovarian follicle development and female fertility. FASEB J 2010; 24:3010–3025.
16. Chen Y, Struhl G. Dual roles for Patched in sequestering and transducing hedgehog. Cell 1996; 87:553–563.
17. Marigo V, Johnson RL, Vortkamp A, Tabin CJ. Sonic hedgehog differentially regulates expression of Gli and Gli3 during limb development. Dev Biol 1996; 180:273–283.
18. Marigo V, Scott MP, Johnson RL, Goodrich LV, Tabin CJ. Conservation in hedgehog signaling: induction of a chicken patched homolog by Sonic hedgehog in the developing limb. Development 1996; 122:1225–1233.
19. Lee J, Platt KA, Censullo P, Ruiz i Altaba A. Gli1 is a target of Sonic hedgehog that induces ventral neural tube development. Development 1997; 124:2537–2552.
20. Ikram MS, Neill GW, Regl G, Eichberger T, Frischauf AM, Aberger F, Quinn A, Philpott M. Gli2 is expressed in normal human epidermis and BCC and induces Gli1 expression by binding to its promoter. J Invest Dermatol 2004; 122:1503–1509.
21. Ingham PW, McMahon AP. Hedgehog signaling in animal development: paradigms and principles. Genes Dev 2001; 15:3059–3087.
22. McGlinn E, Tabin CJ. Mechanistic insight into how Shh patterns the vertebrate limb. Curr Opin Genet Dev 2006; 16:426–432.
23. Dennis G, Sherman BT, Hosack DA, Yang J, Gao W, Lane HC, Lempicki RA. DAVID: Database for Annotation, Visualization, and Integrated Discovery. Genome Biol 2003; 4:P3.
24. Huang DW, Sherman BT, Lempicki RA. Systemic and integrative analysis of large gene lists using DAVID bioinformatcs resources. Nat Protoc 2009; 4:44–57.
25. King P, Paul A, Laufer E. Shh signaling regulates adrenocortical development and identifies progenitors of steroidogenic lineages. Proc Natl Acad Sci U S A 2009; 106:21185–21190.
26. Tian H, Callahan CA, DuPree KJ, Darbonne WC, Ahn CP, Scales SJ, de Sauvage FJ. Hedgehog signaling is restricted to the stromal compartment during pancreatic carcinogenesis. Proc Natl Acad Sci U S A 2009; 106: 4254–4259.
27. Franco HL, Lee KY, Broaddus RR, White LD, Lanske B, Lydon JP, Jeong JW, DeMayo FJ. Ablation of indian hedgehog in the murine uterus results in decreased cell cycle progression, aberrant epidermal growth factor signaling, and increased estrogen signaling. Biol Reprod 2010; 82: 783–790.
28. Risau W. Mechanisms of angiogenesis. Nature 1997; 386:671–674.
29. Byrd N, Grabel L. Hedgehog signaling in murine vasculogenesis and angiogenesis. Trends Cardiovasc Med 2004; 14:308–313.
30. Dyer MA, Farrington SM, Mohn D, Munday JR, Baron MH. Indian hedgehog activates hematopoiesis and vasculogenesis and can respecify prospective neurectodermal cell fate in the mouse embryo. Development 2001; 128:1717–1730.
31. Vokes SA, Yatskievych TA, Heimark RL, McMahon J, McMahon AP, Antin PB, Krieg PA. Hedgehog signaling is essential for endothelial tube formation during vasculogenesis. Development 2004; 131:4371–4380.
32. Astorga J, Carlsson P. Hedgehog induction of murine vasculogenesis is mediated by Foxf1 and Bmp4. Development 2007; 134:3753–3761.
33. Swift MR, Weinstein BM. Arterial-venous specification during development. Circ Res 2009; 104:576–588.
34. Pola R, Ling LE, Silver M, Corbley MJ, Kearney M, Pepinsky RB, Shapiro R, Taylor FR, Baker DP, Asahara T, Isner JM. The morphogen Sonic hedgehog is an indirect angiogenic agent upregulating two families of angiogenic growth factors. Nat Med 2001; 7:706–711.
35. Morrow D, Cullen JP, Liu W, Guha S, Sweeney C, Birney YA, Collins N, Walls D, Redmond EM, Cahill PA. Sonic Hedgehog induces Notch target gene expression in vascular smooth muscle cells via VEGF-A. Arterioscler Thromb Vasc Biol 2009; 29:1112–1118.
36. Lamont RE, Vu W, Carter AD, Serluca FC, MacRae CA, Childs SJ. Hedgehog signaling via angiopoietin1 is required for developmental vascular stability. Mech Dev 2010; 127:159–168.
37. Chen W, Tang T, Eastham-Anderson J, Dunlap D, Alicke B, Nannini M, Gould S, Yauch R, Modrusan Z, Dupree KJ, Darbonne WC, Plowman G, et al. Canonical hedgehog signaling augments tumor angiogenesis by induction of VEGF-A in stromal perivascular cells. Proc Natl Acad Sci U S A 2011; 108:9589–9594.
38. Payne AH, Hales DB. Overview of steroidogenic enzymes in the pathway from cholesterol to active steroid hormones. Endocr Rev 2004; 25: 947–970.
39. Heikkila M, Peltoketo H, Leppaluoto J, Ilves M, Vuolteenaho O, Vainio S.

Wnt-4 deficiency alters mouse adrenal cortex function, reducing aldosterone production. Endocrinology 2002; 143:4358–4365.
40. Merke DP, Bornstein SR, Avila NA, Chrousos GP. NIH conference. Future directions in the study and management of congenital adrenal hyperplasia due to 21-hydroxylase deficiency. Ann Intern Med 2002; 136: 320–334.
41. Val P, Jeays-Ward K, Swain A. Identification of a novel population of adrenal-like cells in the mammalian testis. Dev Biol 2006; 299:250–256.
42. Heikkila M, Prunskaite R, Naillat F, Itaranta P, Vuoristo J, Leppaluoto J, Peltoketo H, Vainio S. The partial female to male sex reversal in Wnt-4-deficient females involves induced expression of testosterone biosynthetic genes and testosterone production, and depends on androgen action. Endocrinology 2005; 146:4016–4023.
43. Jeays-Ward K, Hoyle C, Brennan J, Dandonneau M, Alldus G, Capel B, Swain A. Endothelial and steroidogenic cell migration are regulated by WNT4 in the developing mammalian gonad. Development 2003; 130: 3663–3670.
44. Vainio S, Heikkilä M, Kispert A, Chin N, McMahon AP. Female development in mammals is regulated by Wnt-4 signalling. Nature 1999; 397:405–409.
45. Migone FF, Ren Y, Cowan RG, Harman RM, Nikitin AY, Quirk SM. Dominant activation of the hedgehog signaling pathway alters development of the female reproductive tract. Genesis 2011; 50:28–40.
46. Pazin DE, Albrecht KH. Developmental expression of Smoc1 and Smoc2 suggests potential roles in fetal gonad and reproductive tract differentiaton. Dev Dyn 2009; 238:2877–2890.
47. Barsoum IB, Bingham NC, Parker KL, Jorgensen JS, Yao HHC. Activation of the hedgehog pathway in the mouse fetal ovary leads to ectopic appearance of fetal leydig cells and female pseudohermaphroditism. Dev Biol 2009; 329:96–103.
48. Combes AN, Wilhem D, Davisdson T, Dejana E, Harley V, Sinclair A, Koopman P. Endothelial cell migration directs testis cord formation. Dev Biol 2009; 326:112–120.
49. Lammert E, Cleaver O, Melton D. Induction of pancreatic differentiation by signals from blood vessels. Science 2001; 294:564–567.
50. Matsumoto K, Yoshitomi H, Rossant J, Zaret KS. Liver organogenesis promoted by endothelial cells prior to vascular function. Science 2001; 294:559–563.
51. Ball A, Wenning J, Van Eyk N. Ovarian fibromas in pediatric patients with basal cell nevus (Gorlin) syndrome. J Pediatr Adolesc Gynecol 2011; 24:e5–e7.
52. Raggio M, Kaplan AL, Harberg JF. Recurrent ovarian fibromas with basal cell nevus syndrome (Gorlin syndrome). Obstet Gynecol 1983; 61: 95s–96s.
53. Seracchioli R, Colombo F, Bagnoli A, Trengia V, Venturoli S. Primary ovarian leiomyosarcoma as a new component in the nevoid basal cell carcinoma syndrome: A case report. Am J Obstet Gynecol 2003; 188: 1093–1095.
54. Ismail SM, Walker SM. Bilateral virilizing sclerosing stromal tumours of the ovary in a pregnant woman with Gorlin's syndrome: implications for pathogenesis of ovarian stromal neoplasms. Histopathology 1990; 17: 159–163.